Ionization Energy and Electronic Structure of Polycytidine

J. Magulick,† M. M. Beerbom, B. Lägel, and R. Schlaf*

Department of Electrical Engineering, University of South Florida, Tampa, Florida 33620

Received: July 7, 2005; In Final Form: September 7, 2005

Ribonucleic acid (RNA) polycytidine (poly rC) homopolymer thin films were prepared on highly oriented pyrolytic graphite (HOPG) substrates. The films were grown from aqueous solution directly in a vacuum in multiple steps with use of an electrospray (ES) deposition system. Before poly rC deposition and after each deposition step the sample was characterized with X-ray and ultraviolet photoemission spectroscopy (XPS, UPS). Evaluation of the UP-spectra sequence allowed the determination of ionization energy and highest occupied molecular orbital (HOMO) electronic structure, as well as the charge injection barriers between HOPG and poly rC. Comparison with earlier results on polyadenosine (poly rA) indicates significant differences between ionization energies (poly rC: 8.1 eV; poly rA: 6.8 eV) and orbital alignment at the graphite interface. The larger ionization energy of poly rC results in a larger hole injection barrier and a smaller electron injection barrier relative to the HOPG Fermi level.

Introduction

The electronic structure and in particular the ionization energy of nucleotides has been the focus of experimental and theoretical research for several decades,[1−8] since the electronic properties of these molecules play an important role in deoxyribonucleic acid (DNA) biochemistry. Particularly, DNA damaging processes and carcinogenesis are strongly influenced by the ionization energy of nucleotides.[5,9,10] More recently, motivated by prospects to employ tailor-designed oligonucleotides for the self-assembly of three-dimensional nanostructures,[11−20] the conductivity of nucleotide polymers also has become a widespread research interest. Typically, in conductivity measurements, single nucleotide strands are contacted by using elaborate methods such as scanning probe microscopy or advanced lithographic methods. The results of these measurements have so far been inconsistent, yielding conductive properties ranging from insulating to metallic.[21−25] This suggests that, aside from the particular nucleotide sequence used in the experiment, the contacts between inorganic electrodes and nucleotide strand also play a mayor role in the outcomes of such measurements. Photoemission spectroscopy (PES) offers a way to directly determine charge transfer barriers at interfaces. Gas phase PES allows us to directly measure the highest occupied molecular orbital (HOMO) density of states and ionization energy of single molecules that can be vaporized in a vacuum. PES experiments on molecular thin films also allow the determination of ionization energy, work function, and HOMO density of states in addition to the quantification of the charge injection barriers between the molecules and other materials, as long as the molecules in question can be deposited in situ to avoid environmental contamination.

This has led to a steadily rising number of publications featuring gas phase photoemission spectroscopy (PES) data on ribonucleic acid (RNA) and DNA bases, and their nucleosides. However, gas phase data on nucleotides and their polymers is sparse due to preparatory difficulties (they cannot be evaporated in a vacuum). On the other hand, X-ray photoemission spectroscopy (XPS) measurements on ex situ prepared (dipping, spin coating) nucleotide polymer thin films have been carried out with good success, to determine stoichiometry and film thickness. However, reliable measurements of the highest occupied molecular orbitals (HOMOs) and work function with ultraviolet photoemission spectroscopy (UPS) were difficult to date due to the unavoidable presence of ambient contaminants on the sample surface. Furthermore, the determination of charge injection barriers at nucleotide interfaces with PES has been virtually impossible due to the requirement to perform multistep deposition sequences alternating with PES characterization in situ without breaking the vacuum.[26]

This preparative challenge has recently been addressed through the integration of electrospray deposition into standard ultrahigh vacuum (UHV) equipment, enabling the clean deposition of molecular thin films directly from solution in high vacuum.[27,28] The application of this technique to the deposition of nucleotide polymers is supported by results that suggest that electrospray can be used to deposit thin films of DNA and other materials in the atmosphere without significant fragmentation.[29−34] In general, electrospray is known as a "gentle technique", i.e., it does not result in significant fracturing of molecules, which has led to its wide application in mass spectrometry of large molecules.[35]

In the presented experiments the electronic structure of the polycytidine homopolymer (poly rC) was determined in an experiment where poly rC was deposited in several steps onto an in situ cleaved highly oriented pyrolytic graphite (HOPG) substrate with use of electrospray. After each experimental step the sample surface was characterized by XPS and UPS yielding a series of spectra showing the evolution of the electronic structure from HOPG substrate to poly rC overlayer. HOPG was selected as substrate since it has only very weak valence band emissions allowing observation of the evolution of the poly rC overlayer emissions as the film thickness increases without superposition of significant substrate emissions. Furthermore, HOPG has a high chemical inertness, resulting in only

* Address correspondence to this author. E-mail: schlaf@eng.usf.edu. Fax: 813-974-5250.
† Undergraduate research assistant.

10.1021/jp053722r CCC: $33.50
Published on Web 01/26/2006

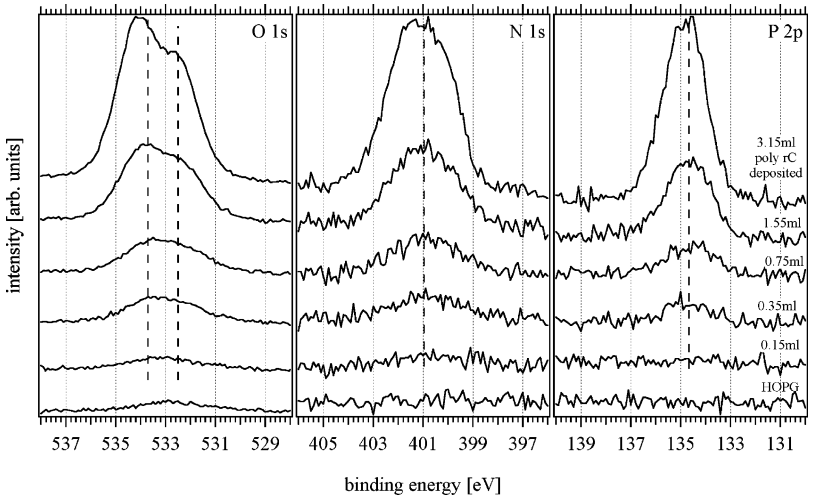

Figure 1. O 1s, N 1s, and P 2p XPS core level spectra measured on vacuum cleaved HOPG and after each poly rC deposition step. Parameter is the injected poly rC solution volume. Charging artifacts are apparent in the shift to higher binding energy after the final deposition step.

minimal disturbance of the overlayer electronic structure by the underlying substrate. Comparison of the presented results with earlier data of a similar experiment investigating the polyadenosine homopolymer/HOPG interface shows that there are significant differences between the nucleotides. In particular, the ionization energy appears to vary strongly, resulting in decidedly different charge injection barriers at interfaces between different nucleotides and electrode materials.

Experimental Section

The experiments were conducted in a commercial ultrahigh vacuum (UHV) system manufactured by SPECS GmbH (Berlin, Germany). The system consists of two preparation chambers, a fast-entry load lock, and a measurement chamber equipped with UPS and XPS. The base pressure of this system is approximately 2×10^{-10} mbar. A home-built electrospray (ES) based deposition system is attached to one of the preparation chambers via two differential pumping stages operating at 0.1 and 4×10^{-3} mbar (for further information about the ES system see ref 27). The ES system can be separated from the deposition chamber by means of a gate valve allowing rapid sample transfer after deposition. The deposition of poly rC (Midland Reagent Company, Inc. minimum length 200 nucleotides, >95% purity) was accomplished by injecting 1 mg/mL of aqueous solution through a 100 μm stainless steel capillary into the intake orifice of the ES system (1 mm diameter) at a rate of 4 mL/h. The capillary was held at a potential of -3.5 kV relative to ground during injection operation. Contamination of ambient air in the vacuum system during ES deposition was reduced to negligible levels by flowing nitrogen at a slight overpressure relative to atmosphere through the capillary mount. The pressure in the deposition chamber rose to about 10^{-5} mbar during deposition.

HOPG substrates (Mikromasch USA, "ZYA" quality) were cleaved in situ to obtain a pristine surface for poly rC deposition. This was accomplished by attaching a thin metal foil with silver epoxy to the top of the HOPG crystal. After loading the sample, a manipulator arm was used to remove the foil along with the top layer of crystal creating a pure, clean graphite surface. The substrate was characterized after cleavage and after each of the five deposition steps by nonmonochromatized XPS and UPS. The substrate was held at room temperature during depositions. The measurements were carried out with a SPECS UVS 10/35 ultraviolet source, and a dual SPECS XR 50 X-ray source (Mg Kα; $h\nu = 1253.6$ eV). UPS measurements were carried out with He I ($h\nu = 21.21$ eV) radiation. A separate sample was prepared for stoichiometry analysis. This experiment was carried out with monochromatized (SPECS FOCUS 500 Ellipsoidal Crystal Monochromator) Al Kα X-ray excitation ($h\nu = 1486.6$ eV,). A -5 V bias was applied during He I and low intensity XPS (LIXPS; for more details on this procedure see ref 36) work function measurements to separate sample and analyzer high binding energy cutoffs, and to increase the emission intensity. Analysis of the photoelectrons was performed with a SPECS Phoibos 100 hemispherical analyzer. The spectrometer was calibrated to yield the standard Cu $2p^{3/2}$ line at 932.66 eV and the Cu $3p^{3/2}$ line at 75.13 eV.[37]

All photoemission spectra were analyzed with Igor Pro (Wavemetrics, Inc.). The work function and HOMO cutoff were determined by fitting a line to each cutoff and calculating the intersect with the binding energy axis. XPS core level spectra were fitted by using a procedure outlined in ref 38. A value of 0.1 eV was added to all cutoff positions to correct for analyzer broadening (determined from the Fermi edge width of 0.2 eV as apparent with particular analyzer settings[39]).

A Digital Instruments (Veeco) Dimension 3000 scanning probe microscope was used to conduct atomic force microscopy (AFM) measurements. Nanoworld cantilevers (resonance frequency 70 kHz, force constant 1.2−5.5 N/m) were used in tapping mode at a scan rate of 1 Hz. The shown data were flattened to eliminate sample tilt.

Results

Spectra for the O 1s, N 1s, and P 2p core level emission lines corresponding to each deposition step are shown in Figure 1. The bottom spectra represent the clean HOPG substrate. While the N 1s and P 2p regions appear flat, a weak O 1s emission at about 532.6 eV is visible. This feature is related to emissions from the sample holder assembly. As the poly rC overlayer increases in thickness, characteristic line shapes related to cytidine appear. The O 1s line appears to consist of three emission features. The most prominent line occurs at 533.6 eV. A second line at about two-thirds the intensity of the first is located at 532.4 eV, and a third, weak feature may be located at about 535 eV. The N 1s line also appears to be composed of at least two emissions of relatively equal intensity at about 400.1 and 401.6 eV. The P 2p line, which only becomes apparent beginning with the 0.35 mL deposition step, is a single peak at an approximate binding energy of 135 eV. All three spectra

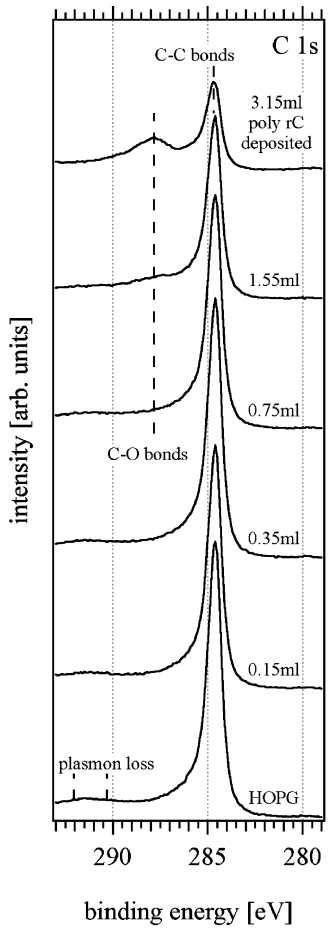

Figure 2. C 1s XPS core level spectra on vacuum cleaved HOPG and after each poly rC deposition step. The emission at ~288 eV is related to C−O bonds from poly rC, while the main peak at 284.7 eV is related to C−C bonds and is related to both substrate and overlayer emissions.

seem to shift to a higher binding energy after the 3.15 mL deposition step, which is indicative of PES charging artifacts.

Figure 2 shows the C 1s spectra for each deposition step. Initially, one prominent line is present at about 284.7 eV, which is characteristic of HOPG and represents C−C bonds. Plasmon loss features are also present at about 291.5 eV. As the deposition volume increases, these features are attenuated while poly rC emissions appear. Additional emission features at about 288 eV become apparent after the 1.55 mL deposition step.

The corresponding UPS spectra for each experimental step are shown in Figure 3. The full spectra are shown in the center. These spectra contain three main regions. Between 0 eV and about 9 eV HOPG valence bands and poly rC HOMO emissions occur. At higher binding energies the background of inelastically scattered electrons becomes dominant. The prominent emission at 13.6 eV is characteristic of electrons that are inelastically scattered into a high density of states region of the HOPG conduction bands. The high binding energy cutoff of the spectra allows determination of the sample work function. The graph on the right in Figure 3 shows the spectra of the valence bands/HOMO region with the background removed in more detail. The main feature at about 8.5 eV and the weaker features at about 5 and 3 eV in the bottom spectrum correspond to HOPG valence band emissions. As the poly rC layer thickness increases, HOMO emissions emerge between about 3 and 12 eV. A shift due to charging artifacts occurs in these features as the layer grows thicker. The shift becomes apparent after the 0.75 mL deposition step, as opposed to the XPS data where shifts become apparent only after 3.15 mL. The reason for this is the much weaker photon flux in XPS measurements compared to UPS, which therefore requires a thicker (less conductive) layer to cause charging artifacts.

The graph on the left shows the high binding energy cutoff normalized for better comparison of the cutoff energies. A shift of the cutoff is apparent immediately after the first deposition step, and becomes more pronounced as deposition volume increases. This shift also corresponds to charging artifacts, as was determined from LIXPS measurements performed before UPS (not shown), where the cutoff did not shift at all, indicating the absence of an interface dipole or band bending.

Figure 4 shows AFM images of $5 \times 5\ \mu m^2$ areas measured on a cleaved HOPG substrate (left) and the 3.15 mL poly rC thin film on HOPG (right). The graph on the bottom represents the two cross sections of the cleaved HOPG and poly rC thin film as indicated in the corresponding images. The black to white height scale is 40 nm in both images. The HOPG cross section shows the typical steps of graphite layers characteristic of HOPG with a total variation of about 5 nm in height. Strand-like features are present on the poly rC film layer with heights that vary from 5 to 10 nm and widths of up to 150 nm.

Discussion

(A) Stoichiometry. The insert in Figure 3 shows the structure of poly rC. There are 7 oxygen, 3 nitrogen, 1 phosphorus, and 9 carbon atoms per nucleotide. An analysis of the corresponding peak intensities of the atomic species should approximate these ratios within experimental error. Figure 5 shows the fits to the O 1s, N 1s, C 1s, and P 2p emission regions, which were measured with monochromated X-rays on a separate 3.15 mL poly rC layer corresponding to the last deposition step in the deposition series.

The O 1s spectrum at the top of Figure 5 shows at least three distinct emissions. The fitted lines have maxima at 532.5, 534.2, and 535.7 eV, and identical full width at half-maxima (fwhm) values of 1.81 eV. The two main peaks are related to the poly rC overlayer, while the small peak at 535.7 eV is probably related to a small amount of coadsorbed water, similar to what was found on poly rA films in earlier experiments.[28] Two of the oxygen atoms are directly bonded to phosphorus, and one is double bonded to a carbon in the nitrogenous base, while the other four are bonded to two carbons in the ribose sugar, and to a carbon and phosphorus atom between the sugar and the phosphate. This allows an assignment of the more prominent peak to the emissions from C−O−C structures, which occur at a range from 532.94 to 533.59 eV,[40] and C−O−P structures, which occur at 533.37 eV.[40] This leaves the secondary peak to be assigned to the oxygen atoms in the phosphate, which emit in a range from 530.5 to 532.5 eV,[41] and the double bonded oxygen in the base, which appears around 532.3 eV.[40] The intensity ratio between the fitted main and secondary peaks was determined to be 1.39:1, in close agreement with the theoretical ratio of 1.33:1 (4:3).

The fit to the N 1s emissions is shown in the second graph from the top in Figure 5. The fit was performed with two lines appearing at 400.5 and 402.0 eV with full width at half maxima (FWHMs) of 1.88 and 1.95 eV, respectively. When examining the bonding of the nitrogen atoms in the poly rC structure, two N atoms seem to be in similar environments, each part of the pyrimidine ring. The third N atom exists in an $-NH_2$ substituent. Comparison with other XPS results on immobilized oligonucleotides shows that the N 1s emissions from a nonconjugated pyrimidine ring occur at about 401 eV.[42] From measurements

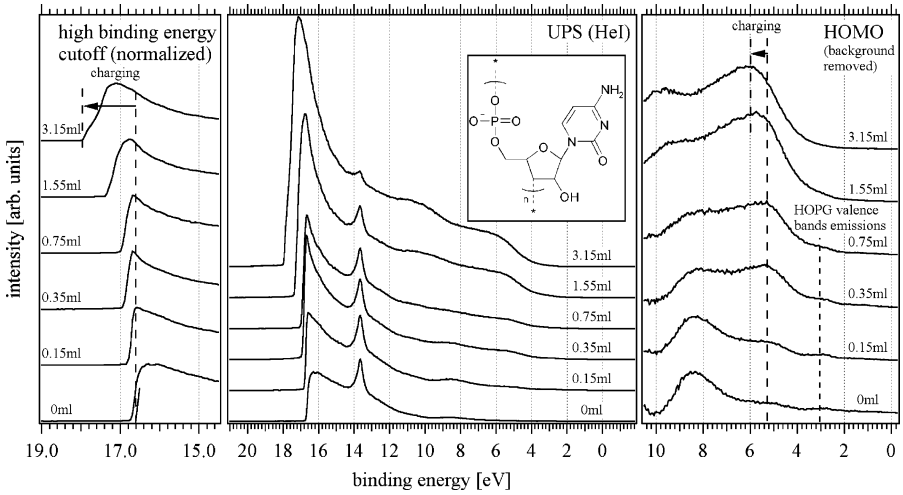

Figure 3. UP spectra corresponding to XPS data shown in Figures 1 and 2. The full spectra are shown in the center. As film thickness increases emissions from the highest occupied molecular orbitals (HOMOs) of poly rC become apparent between 3 and 12 eV. The development of the HOMO emissions is shown with background removed on the right. In the left, the secondary edge is shown normalized. The shift to higher binding energy is related to the occurrence of charging artifacts.

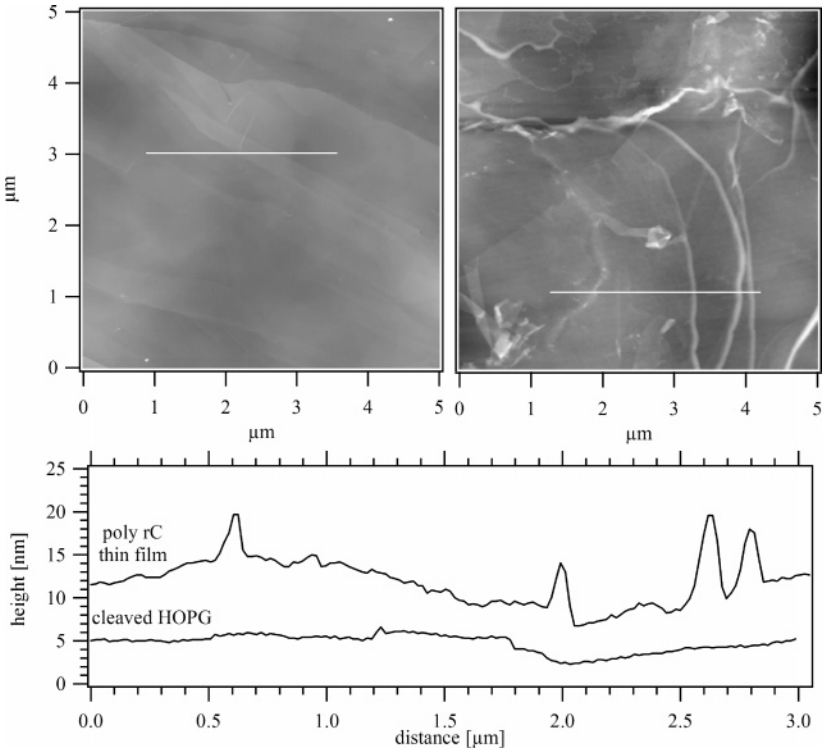

Figure 4. Topographs of tapping mode atomic force microscopy of a cleaved HOPG surface (left) and after the final 3.15 mL of poly rC deposition step (right). Each image represents an area of $5 \times 5\ \mu m^2$. The left graph shows typical graphene sheet related steps. Rope-like features are observed on the poly rC thin film. The graph at the bottom shows line scans corresponding to the white lines drawn on the images.

of $-NH_2$ ligands,[43] N 1s emissions from these groups are known to be located at about 400 eV, which matches well the position of the lower binding energy line. However, the intensity ratio between the peaks, which is 1.23:1, is distinctly different from the stoichiometric ratio of 2:1, which cannot be explained by peak fitting ambiguities alone. It is interesting to note that a similar phenomenon was observed on poly rA thin films in a similar experiment.[28] At this point it remains unclear as to why this phenomenon occurs, and further investigation is needed.

The C 1s fit is shown in the second graph from the bottom in Figure 5. Since the spectrum contains significant emissions from the graphite substrate, only emissions that are not C−C related can be analyzed in a similar fashion as the other peaks. The C 1s spectrum was fitted with four single lines at 284.7, 286.0, 288.1, and 290.0 eV with FWHMs of 0.7, 1.86, 1.97, and 1.90 eV respectively. Comparison with the poly rC structure allows the following assignments of the lines: The most prominent peak at 284.7 eV corresponds to C−C bonds, i.e., can be attributed to emissions from the substrate and the one carbon in the pyrimidine ring, which is bound to two other carbons. The two peaks at intermediate binding energies represent carbons bound to nitrogen in the pyrimidine ring, and carbons bound to oxygen in the ribose substituent. XPS measurements on nucleotides immobilized on gold found binding energies for carbons in the ribose and pyrimidine ring to occur at 286−287 for C−N bonds and ∼286.5 for C−O bonds,[44] making it difficult to assign each peak to a single one of these species. The high binding energy peak can be assigned

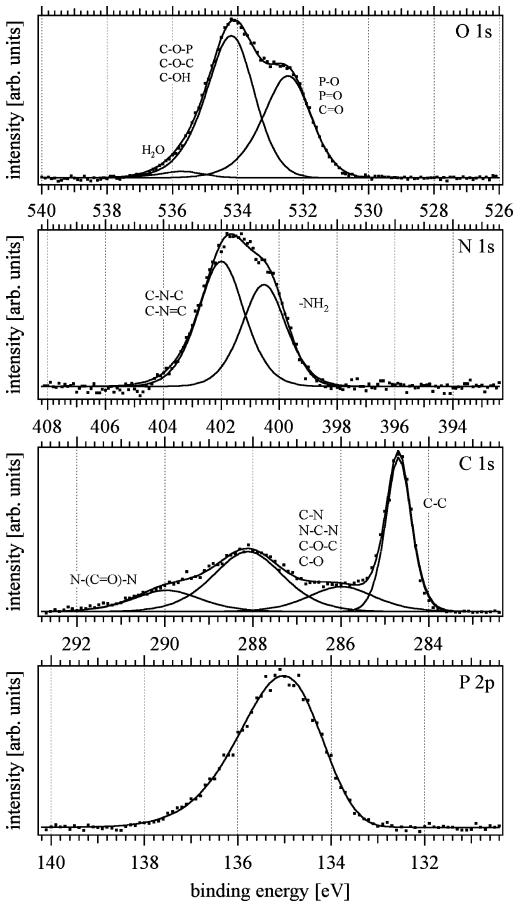

Figure 5. O 1s, N 1s, C 1s and P 2p spectra (dotted lines) measured with monochromatized Al Kα radiation after deposition of 3.15 mL of poly rC solution. Full lines: Gaussian−Lorenzian peaks fitted to the emission lines.

to the carbonyl.[44] It is interesting to point out that the binding energies found in the presented experiment are consistently about 1 eV higher than those given in ref 44. This discrepancy may be related to calibration differences or the formation of an interface dipole between Au and poly rC, which would result in a shift of the poly rC spectra relative to the Au Fermi level.

The bottom graph of Figure 5 shows the fit to the P 2p line, which was performed by using a single 2:1 intensity ratio doublet, as expected for p-orbital related emissions from atoms in identical bonding environments (only one P atom per nucleotide). From this analysis, the P $2p^{3/2}$ and $2p^{1/2}$ positions were determined to be at 134.8 and 135.6 eV, respectively.

By using the fitted curves, a peak area analysis was performed to find the relative intensities between the emissions of each atomic species, using the same approach as outlined in ref 28.

The used parameters, and calculated values of normalized intensities with respect to P 2p, are shown in Table 1. The relative intensity ratios between P 2p and N 1s (1:2.2) and O 1s (1:6.1) are somewhat lower than theoretical values (3:1 and 7:1 respectively), but fall within typical accuracy of PES stoichiometry analysis (∼10−20% if no standards are used). Our results are also confirmed by area analysis of cytosine DNA oligomers by May et al.,[44] where ratios for O 1s and N 1s relative to P 2p were also found to be slightly lower (5.93:1 for O 1s and 2.5:1 for N 1s) than the stoichiometric values. The relative measured intensity ratio for the non-C−C bonded carbon atoms of 7.6:1 compares well to the stoichiometric ratio of 8:1 between the carbons in N−C−N, C−N, C−O, and N−(C═O)−N environments and phosophorus.

(B) Interface Morphology. A frequently used procedure to estimate thin film thickness from PES data is to take a core level emission unique to the substrate and evaluate its attenuation as the deposition progresses. However, this is not easily possible in the presented measurements since the C 1s emission from the substrate is superimposed by emissions from the poly rC overlayer. The only substrate unique emission is the feature at about 13.6 eV in the UP spectra. The sequence of this feature is shown in Figure 6 with the background removed. This emission clearly diminishes as deposition progresses. Its attenuation allows estimation of the thickness of the deposited layer. The result of this approach is shown in Figure 7 where film thickness is graphed versus the injected volume of poly rC solution. The thickness values were estimated by using an exponential decay function describing the attenuation of substrate emissions due to the deposited film:

$$I = I_0 \exp\left(-\frac{d}{\mathrm{MFP}}\right) \tag{1}$$

In this equation, I is the measured intensity of the substrate related emission feature, MFP corresponds to the mean free path of the emitted electrons, and d is the desired thickness. Solving the equation for d, one obtains:

$$d = -\mathrm{MFP} \ln\left(\frac{I}{I_0}\right) \tag{2}$$

It should be pointed out that absolute values obtained for d with this method probably have an error in the range of −50% to +100% since a MFP value determined for carbon[45] was used (the MFP in oligonucleotides appears not to be published to date). Furthermore, eq 1 requires a homogeneous layer thickness across the sample surface, which is not met by our samples. Nonetheless, the method allows obtaining an estimate of the thickness. The evaluation of the calculated thickness curve yields an increase of the film thickness during the first deposition steps at an estimated rate of about 50 Å/mL. After the third deposition step the curve continues at a slope of 25 Å/mL, indicating the formation of 3-D features.[46] This Stranski−Krastanov like growth mode is confirmed by the AFM images shown in Figure 4. Most of the area appears flat, although rope-like strands (∼150 nm across) are present that are dispersed across the surface. Analysis of the topographs yielded that about 4% of the area is covered by the rope-like features, allowing the conclusion that the PE spectra were not significantly affected by rope related emissions.

(C) Electronic Structure. Determination of the electronic structure of the interface between HOPG and poly rC was accomplished by analyzing the HOMO emissions in the UP spectra. In the presented system, charging artifacts must be considered since LIXPS measurements carried out before UPS measurements did not indicate any significant shifts of the spectra as the poly rC layer increased in thickness. Therefore, it has to be concluded that the UPS cutoff is already affected by charging artifacts after the first deposition step. In comparison, the HOMO maximum appears to remain at the same position up to the 0.75 mL step. This difference is related to the fact that the cutoff feature is affected differently by charging. While the cutoff is dominated by the slowest electrons, primary peaks such as the HOMO features represent a true average of the emissions of the whole surface. Hence, the occurrence of charging artifacts on a small area may already have a strong effect on the cutoff, while primary peaks only show a weak shift related to increased emissions on the high binding energy

TABLE 1: Values Used To Calculate Absolute Peak Intensities for Stoichiometric Evaluation

	peak area (*A*)	cross section (CS)	mean free path (MFP), Å	kinetic energy (E_{kin}), eV	transmission factor (TF)	normalized absolute intensity ($I_{absolute}$)[a]
N1s	941	1.8	28	1086	0.030	2.2
O1s	4269	2.93	26	956	0.032	6.1
P2p	312	1.18	34	1351	0.027	1.0
C1s (C−O, C−N)[b]	1985	1.0	31	1202	0.029	7.6

[a] Absolute intensities are given normalized relative to the P 2p peak area. [b] The C1s peak area and relative intensity values includes only C−N, N−C−N, C−O, and N−(C═O)−N emissions due to superimposed substrate emissions on the C−C related peak.

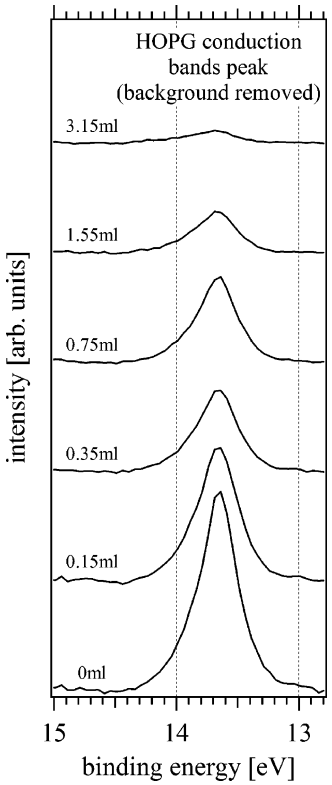

Figure 6. UPS emission feature at 13.7 eV binding energy with background removed. The attenuation of this feature was used for poly rC overlayer thickness calibration.

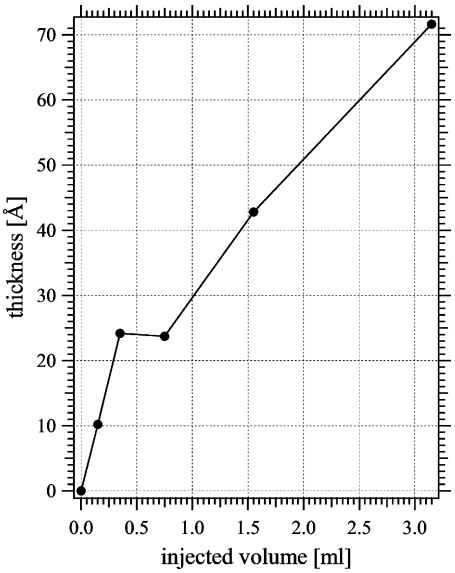

Figure 7. Thickness vs injected solution volume. The initial deposition rate amounts to about 28 Å/ml.

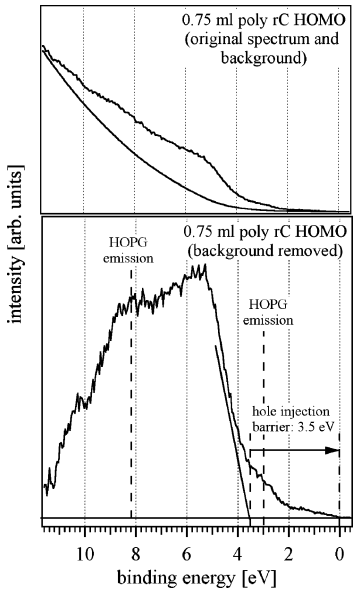

Figure 8. Determination of hole injection barrier at the HOPG/poly rC interface. The top graph shows the original UP spectrum measured after the 0.75 mL deposition step with fitted background. The spectrum after background removal is shown at the bottom. The cutoff was determined to be at about 3.5 eV by fitting a line to the onset of the main peak feature. The weak shoulder at 3 eV represents an emission feature related to the HOPG substrate.

side of the peak. In fact, peak onset binding energies on the low binding energy side should not be affected by charging at all, as long as there is still a not-charging-affected area on the surface contributing to the spectrum. On the basis of this reasoning, the 0.75 mL spectrum was selected for the HOMO onset determination, since no significant charging related shifts are observed in the HOMO peak positions.

The analysis of the 0.75 mL HOMO spectrum is shown in Figure 8. The original spectrum is shown at the top with a line fitted to the background signal. The background was determined by fitting the integral of the spectrum[47] to the regions around the HOMO emissions. The spectrum with the background removed is shown on the bottom where three significant emission features are visible. The emission at a binding energy of ~8 eV originates from the HOPG substrate. Poly rC HOMO emissions occur at lower binding energy and consist of a prominent main peak at about 5.5 eV. The emission shoulder at around 3 eV is also related to HOPG. This is evident from the feature's complete attenuation after the final deposition steps (compare Figure 3). The HOMO cutoff was determined by fitting a line to the low binding energy side of the HOMO peak, and finding the intersect with the binding energy axis. This is shown schematically in the bottom graph of Figure 8. From this procedure the hole injection barrier (Φ_h) between HOPG and poly rC was determined to be 3.5 eV (this value was corrected by adding 0.1 eV to account for the analyzer resolution).

From the LIXPS cutoff features, which did not show any shifts (similar to the data shown in ref 28), it can further be

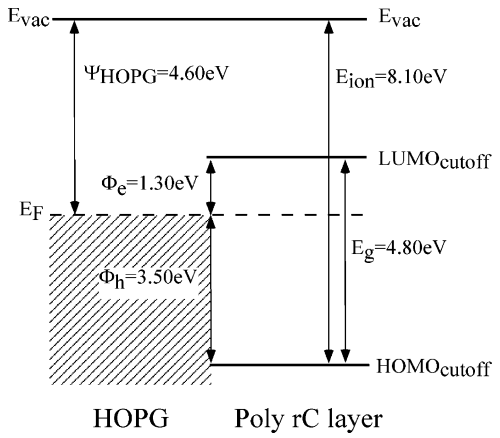

Figure 9. Schematic depiction of the orbital line-up at the poly rC/HOPG interface as determined from the PE spectra sequences. The interface shows significant charge injection barriers. The ionization energy of the poly rC layer was found to be 8.1 eV.

concluded that no interface dipole was formed at the HOPG/poly rC interface. This is supported by other experiments on HOPG/organic molecule interfaces[48,49] where no dipoles were found. Furthermore, the high chemical inertness of HOPG usually results in the formation of van der Waals bonds with organic materials, rather than chemical bonds (which would give rise to interface dipoles).

The electron injection barrier (Φ_e) can be estimated by using the HOMO − lowest unoccupied molecular orbital (LUMO) gap (E_g). Using an E_g value of 4.8 eV as determined by UV absorption,[50] the electron injection barrier (Φ_e) between the Fermi level of HOPG and poly rC LUMO was estimated to be 1.3 eV. However, this value should be regarded only as a lower margin of this energy barrier, since optical gap measurements include exciton features, which can amount to several tenths of an electronvolt in organic materials.[51] The work function of the clean HOPG substrate was determined to be 4.60 eV by subtracting the binding energy of the high binding energy cutoff of the initial UP spectrum from the excitation energy of the He I line, 21.21 eV. Adding the hole injection barrier (Φ_h) and the HOPG work function, a value for the ionization energy of poly rC can be obtained, which was determined to be 8.10 eV.

The above evaluation is summarized in Figure 9 where a schematic of the orbital alignment is shown. The large charge injection barriers suggest poor charge transfer across this interface in both directions, which is supported by the observed charging artifacts occurring already at the initial deposition steps. It is interesting to compare the orbital alignments of poly rC and poly rA. Poly rA has a significantly smaller ionization energy of 6.8 eV (note that this value was misstated as "7.8 eV" in ref 28) than poly rC. This suggests that the ionization energy is defined by orbitals on the bases rather than on the backbone, which is supported by gas phase PES data and theoretical calculations by LeBreton and co-workers: Spectral comparison between UPS data of model compounds related to uracil, ribose, and uridine clearly indicate that the HOMO emissions of uridine originate mainly from uracil.[3] This was later confirmed by ab initio calculations on adenine and adenosine where it was concluded that the ribose and phosphate related ionization potentials are larger than that of adenine.[6]

With regard to the observed ionization energy difference of 1.3 eV between poly rA and poly rC, it appears that most theoretical and experimental studies agree qualitatively with the findings presented here; however, quantitatively, there are differences. Gas phase PES measurements by LeBreton et al. yielded 8.39 eV as the ionization potential of methyladenine,[6] 8.65 eV for methylcytosine, and about 9.0 eV for cytosine.[2] The latter value agrees well with an earlier gas phase PES measurement by Dougherty et al., who also found a HOMO position close to 9.0 eV.[7] Photoionization mass spectrometry measurements by Orlov et al. yielded similar values stating a 0.4 eV difference between adenine and cytosine.[1] Theoretical calculations by Russo et al. also indicate that adenine has an about 0.5 eV smaller ionization energy than cytosine. The reason for the smaller differences may lie in the significantly different situation in our measurements, where thin films on graphite substrates have been characterized, while the above results were obtained on isolated molecules in the gas phase. Furthermore, our measurements are probably fraught with an error of about ±0.2 eV with regard to absolute binding energy positions due to the fitting procedure, and the broad shape of the HOMO emissions, which are superimposed by HOPG valence band emissions.

These findings imply that it is of crucial importance for conductivity measurements on oligomer strands on what nucleotide the contact is made and, perhaps, which part of the molecule is actually involved in the interaction with the electrode. Further experiments are needed in which the injection barriers to the remaining nucleotides (poly rU, rG, rT), the backbone, and isolated nucleosides and bases are determined individually, as well as theoretical calculations of the density of states of nucleotides, which would allow us to directly assign the observed HOMO related emission features to molecular states.

Conclusion

Polycytidine (poly rC) homopolymer was deposited on highly ordered pyrolytic graphite (HOPG) with electrospray deposition in a vacuum. The deposition was carried out in several steps without breaking the vacuum. Photoemission spectroscopy (PES) characterization with ultraviolet and X-ray excitation (UPS, XPS) before deposition and after each deposition step allowed the determination of the charge injection barriers between HOPG and poly rC, and the determination of the ionization energy of poly rC. Stoichiometry analysis based on core level peak intensities yielded good agreement with previous experiments where nucleotide thin films were prepared ex situ. The electronic structure of the interface is characterized by large charge injection barriers and the absence of an interface dipole. The ionization energy was found to be 8.1 eV, considerably larger than what was found earlier on similarly prepared polyadenosine (poly rA) thin films (6.8 eV).

Acknowledgment. Financial support by the National Science Foundation (grant DMR 0205577) is gratefully acknowledged. J.M. acknowledges partial funding through Engineering Undergraduate Research Fellowships provided by the USF College of Engineering Research Experience for Undergraduates program.

References and Notes

(1) Orlov, V. M.; Smirnov, A. N.; Varshavsky, Y. M. *Tetrahedron Lett.* **1976**, *48*, 4377−4378.

(2) Yu, C.; Peng, S.; Akiyama, I.; Lin, J.; Lebreton, P. R. *J. Am. Chem. Soc.* **1978**, *100* (8), 2303−2307.

(3) Yu, C.; Odonnell, T. J.; Lebreton, P. R. *J. Phys. Chem.* **1981**, *85* (25), 3851−3855.

(4) Close, D. M. *J. Phys. Chem. A* **2004**, *108* (46), 10376−10379.

(5) Fernando, H.; Papadantonakis, G. A.; Kim, N. S.; LeBreton, P. R. *Proc. Natl. Acad. Scie. U.S.A.* **1998**, *95* (10), 5550−5555.

(6) Kim, N. S.; Jiang, Q.; Lebreton, P. R. *Int. J. Quantum Chem.* **1996**, *60* (8), 11−19.
(7) Dougherty, D.; McGlynn, S. P. *J. Chem. Phys.* **1977**, *67* (3), 1289−1290.
(8) Russo, N.; Toscano, M.; Grand, A. *J. Comput. Chem.* **2000**, *21* (14), 1243−1250.
(9) Wesolowski, S. S.; Leininger, M. L.; Pentchev, P. N.; Schaefer, H. F. *J. Am. Chem. Soc.* **2001**, *123* (17), 4023−4028.
(10) Saito, I.; Nakamura, T.; Nakatani, K.; Yoshioka, Y.; Yamaguchi, K.; Sugiyama, H. *J. Am. Chem. Soc.* **1998**, *120* (48), 12686−12687.
(11) Chen, J. H.; Seeman, N. C. *Nature* **1991**, *350* (6319), 631−633.
(12) LaBean, T. H.; Yan, H.; Kopatsch, J.; Liu, F. R.; Winfree, E.; Reif, J. H.; Seeman, N. C. *J. Am. Chem. Soc.* **2000**, *122* (9), 1848−1860.
(13) Mao, C. D.; Sun, W. Q.; Seeman, N. C. *J. Am. Chem. Soc.* **1999**, *121* (23), 5437−5443.
(14) Mao, C. D.; Sun, W. Q.; Seeman, N. C. *Nature* **1997**, *386* (6621), 137−138.
(15) Nielsen, P. E.; Egholm, M.; Berg, R. H.; Buchardt, O. *Science* **1991**, *254* (5037), 1497−1500.
(16) Robinson, B. H.; Seeman, N. C. *Protein Eng.* **1987**, *1* (4), 295−300.
(17) Seeman, N. C. *Nano Lett.* **2001**, *1* (1), 22−26.
(18) Yan, H.; Zhang, X. P.; Shen, Z. Y.; Seeman, N. C. *Nature* **2002**, *415* (6867), 62−65.
(19) Yurke, B.; Turberfield, A. J.; Mills, A. P.; Simmel, F. C.; Neumann, J. L. *Nature* **2000**, *406* (6796), 605−608.
(20) Winfree, E.; Liu, F. R.; Wenzler, L. A.; Seeman, N. C. *Nature* **1998**, *394* (6693), 539−544.
(21) Fink, H. W.; Schonenberger, C. *Nature* **1999**, *398* (6726), 407−410.
(22) Porath, D.; Bezryadin, A.; de Vries, S.; Dekker, C. *Nature* **2000**, *403* (6770), 635−638.
(23) Cuniberti, G.; Craco, L.; Porath, D.; Dekker, C. *Phys. Rev. B* **2002**, *65* (24), art. no. 241314(R).
(24) Storm, A. J.; van Noort, J.; de Vries, S.; Dekker, C. *Appl. Phys. Lett.* **2001**, *79* (23), 3881−3883.
(25) Cai, L. T.; Tabata, H.; Kawai, T. *Appl. Phys. Lett.* **2000**, *77* (19), 3105−3106.
(26) Waldrop, J. R.; Grant, R. W. *Phys. Rev. Lett.* **1979**, *43* (22), 1686−1689.
(27) Dam, N.; Beerbom, M. M.; Braunagel, J. C.; Schlaf, R. *J. Appl. Phys.* **2005**, *97* 024909.
(28) Dam, N.; Doran, B. V.; Braunagel, J. C.; Schlaf, R. *J. Phys. Chem.* **2005**, *109* (2), 748−756.
(29) Vanderei, W.; Oldenhof, W.; Zehner, W. *Nucl. Instrum. Methods* **1973**, *112* (1−2), 343−351.
(30) Lowentha, Gc.; Wyllie, H. A. *Nucl. Instrum. Methods* **1973**, *112* (1−2), 353−357.
(31) Lauer, K. F.; Verdingh, V. *Nucl. Instrum. Methods* **1963**, *21* (1), 161−166.
(32) Morozov, V. N.; Morozova, T. Y. *Anal. Chem.* **1999**, *71* (15), 3110−3117.
(33) Festag, R.; Alexandratos, S. D.; Joy, D. C.; Wunderlich, B.; Annis, B.; Cook, K. D. *J. Am. Soc. Mass Spectrom.* **1998**, *9* (4), 299−304.
(34) Festag, R.; Alexandratos, S. D.; Cook, K. D.; Joy, D. C.; Annis, B.; Wunderlich, B. *Macromolecules* **1997**, *30* (20), 6238−6242.
(35) Cole, R. B. *Electrospray Ionization Mass Spectrometry*: *Fundamentals, Instrumentation, and Applications*; John Wiley & Sons: New York, 1997.
(36) Schlaf, R.; Merritt, C. D.; Crisafulli, L. A.; Kafafi, Z. H. *J. Appl. Phys.* **1999**, *86* (10), 5678−5686.
(37) Seah, M. P. *Surf. Interface Anal.* **1989**, *14*, 488.
(38) Kojima, I.; Kurahashi, M. *J. Electron. Spectrosc. Relat. Phenom.* **1987**, *42*, 177.
(39) Kohlscheen, J.; Emirov, Y. N.; Beerbom, M. M.; Wolan, J. T.; Saddow, S. E.; Chung, G.; MacMillan, M. F.; Schlaf, R. *J. Appl. Phys.* **2003**, *94* (6), 3931−3938.
(40) Briggs, D.; Beamson, G. *Anal. Chem.* **1993**, *65* (11), 1517−1523.
(41) Moulder, J. F.; Stickle, W. F.; Sobol, P. E.; Bomben, K. D. *Handbook of X-ray Photoelectron Spectroscopy*; Physical electronics, Inc.: Eden Prairie, MI, 1995.
(42) Saprigin, A. V.; Thomas, C. W.; Dulcey, C. S.; Patterson, C. H.; Spector, M. S. *Surf. Interface Anal.* **2005**, *37* (1), 24−32.
(43) Jones, T. S.; Ashton, M. R.; Richardson, N. V.; Mack, R. G.; Unertl, W. N. *J. Vac. Sci. Technol. A* **1990**, *8* (3), 2370−2375.
(44) May, C. J.; Canavan, H. E.; Castner, D. G. *Anal. Chem.* **2004**, *76* (4), 1114−1122.
(45) Tilinin, I. S.; Jablonski, A.; Werner, W. S. M. *Prog. Surf. Sci* **1996**, *52* (4), 193−335.
(46) Argile, C.; Rhead, G. E. *Surf. Sci. Rep.* **1989**, *10*, 277−356.
(47) Riggs, W. M.; Parker, M. J. Surface analysis by X-ray photoelectron spectroscopy. In *Methods of Surface Analysis*; Czanderna, A. W., Ed.; Elsevier Publishing Company: Amsterdam, The Netherlands, 1975; pp 103−158.
(48) Schlaf, R.; Parkinson, B. A.; Lee, P. A.; Nebesny, K. W.; Armstrong, N. R. *Surf. Sci.* **1999**, *420* (1), L122−L129.
(49) Schroeder, P. G.; France, C. B.; Parkinson, B. A.; Schlaf, R. *J. Appl. Phys.* **2002**, *91* (11), 9095−9107.
(50) Petrovykh, D. Y.; Kimura-Suda, H.; Tarlov, M. J.; Whitman, L. J. *Langmuir* **2004**, *20* (2), 429−440.
(51) Pope, M.; Swenberg, C. E. *Electronic Processes in Organic Crystals and Polymers*; Oxford University Press: Oxford, UK, 1999.